Mechanism and Machine Theory 100 (2016) 138–154

Contents lists available at ScienceDirect

Mechanism and Machine Theory

journal homepage: www.elsevier.com/locate/mechmt

A new design methodology for four-bar linkage mechanisms based on derivations of coupler curve

Jong-Won Kim [a], TaeWon Seo [b,*], Jongwon Kim [a,**]

[a] School of Mechanical and Aerospace Eng., Seoul Nat'l Univ., 151-019, Republic of Korea
[b] School of Mechanical Eng., Yeungnam Univ., 712-749, Republic of Korea

ARTICLE INFO

Article history:
Received 3 March 2015
Received in revised form 10 February 2016
Accepted 11 February 2016
Available online 4 March 2016

Keywords:
Four-bar linkage
Mechanism synthesis
Coupler curve classification
Design optimization

ABSTRACT

This paper presents a new design methodology for crank-rocker four-bar linkages based on differential objective functions. Firstly, to avoid obtaining a mechanism with an unintended trajectory shape, we classified the trajectory of the linkage into four types of shapes. Two-step optimization for a specific shape type is proposed. In the first step, the shape of the trajectory is obtained by minimizing the root mean square error (RMSE) between the slope (first-order derivative) of the coupler point and that of the target trajectory. The size of the trajectory is then determined by minimizing the RMSE between the change in angle of slope (second-order derivative) of the coupler point and that of the desired trajectory. This new approach has three advantages: i) the desired trajectory can be set as a continuous and closed loop, ii) the optimal solution can be obtained without the possibility of generating a mechanism with an unintended coupler curve, and iii) the method can take account of the velocity of the output for each section with a constant input velocity. Three case studies were conducted to verify the advantages of the new approach based on a new index called the goodness of traceability.

1. Introduction

Four-bar linkages are widely used in mechanical devices due to their simple structure, ease of manufacturing, and low cost. The path synthesis of planar four-bar linkages has been studied with a variety of methods during the past 60 years [1–7]. The methods in these studies can be classified as graphical, analytical, or numerical.

Hrones and Nelson used a graphical method that involves an atlas of coupler curves [1]. They developed a four-bar linkage atlas with almost 7000 coupler curves. Similarly, Zhang et al. [8] proposed an atlas of five-bar geared linkage coupler curves. Alternatively, other graphical methods involve drawing by hand [9]. Graphical methods are quick and straightforward, but the accuracy of these approaches is limited due to drawing error, which can be critical for the design of precision mechanical devices. Also, because of the complexity of obtaining solutions with a reasonable result, the geometric construction may have to be repeated many times.

Analytical approaches were first addressed by Sandor [2] and by other researchers thereafter [10,11]. Methods for finding suitable four-bar linkages that can precisely trace desired precision points analytically have been developed, and the number of desired precision points has increased from four to nine. Once a mechanism is modeled mathematically and coded for a computer simulation, parameters such as the lengths of each link are easily handled to create new solutions without further programming. However, there is no analytical solution to the general problem of four-bar linkage synthesis for more than nine target points.

* Corresponding author. Tel.: +82 53 810 2442; fax: +82 53 810 4627.
** Corresponding author. Tel.: +82 2 880 7144; fax: +82 2 875 4848.
E-mail addresses: taewon_seo@yu.ac.kr (T. Seo), jongkim@snu.ac.kr (J. Kim).

http://dx.doi.org/10.1016/j.mechmachtheory.2016.02.006
0094-114X/

Thus, this methodology cannot be applied for the design of four-bar linkages whose coupler point can trace a large number of target points or continuous and closed loops. This problem may be solved using a numerical method.

There are two types of numerical method. One is using numerical atlas database of coupler curve with Fourier series method [12,13,14]. The other method is optimizing parameters to minimize an objective function, and obtain the solution numerically. The most widely used objective function is the tracking error (TE), which is defined as the sum of the square of the Euclidean distance between the desired points and the obtained coupler points. To the best of our knowledge, the first to address this objective function was Han [3]. Due to the ease of calculation, TE has been used in various studies [5,15,16]. However, using TE for the objective function could generate unintended trajectory shapes. Furthermore, when the input angular velocity is constant, it is not easy to take account of the velocity of the coupler point that traces the trajectory of the four-bar linkage.

To overcome these disadvantages, this paper introduces a new numerical approach for the design of a four-bar linkage. Classifications are also presented for the possible trajectory shapes of a crank-rocker four-bar linkage: elliptical, semi-elliptical, crescent, and intersectional. These classifications were used to figure out the first and second-order derivatives (slope and change in angle of slope) of the coupler point, which reflect the characteristics of each shape type and the size of the entire trajectory. The root-mean-square error (RMSE) of these derivative values between the desired and obtained trajectories is used as the objective function.

This method has three advantages compared to conventional numerical approaches. First, using the derivative of the trajectory, which is a continuous function, the desired trajectory can be set as a continuous and closed loop. In contrast, methods that minimize TE require points for the desired trajectory. Second, if the four-bar linkage is designed to follow the derivative value profile according to the input angle, the method can obtain the optimal solution without the possibility of generating an unintended shape. Finally, by adjusting the interval of two peak points of the derivative profile of the desired trajectory, the method can take account of the velocity of each section of the coupler curve with constant input velocity.

The performance of the numerical method was investigated using a new index called the goodness of traceability (GT). GT is defined as TE as a function of the input angle of the four-bar linkage. This allows the shape and velocity to be considered simultaneously. GT can be used to compare the performance of each method objectively.

This paper is organized as follows. The trajectory classification of the four-bar linkage is presented in Section 2. Section 3 presents the new design method, and Section 4 presents the performance of the method in comparison to a conventional method. The GT index is also demonstrated in this section. Discussions and a conclusion are given in Section 5 and Section 6, respectively.

2. Classification of trajectories of crank-rocker four-bar linkage coupler point

The trajectories of the coupler point of a crank-rocker four-bar linkage need to be classified to gain insight about them. The shape classifications are explained, and the mathematical properties of each shape type are described.

2.1. Coupler point of crank-rocker four-bar linkage

To form a crank-rocker four-bar linkage, the relationships between each link length need to satisfy the Grashof conditions [17]:

$$T_1 = l_4 + l_2 - l_1 - l_3 > 0 \tag{1a}$$

$$T_2 = l_3 + l_4 - l_1 - l_2 > 0 \tag{1b}$$

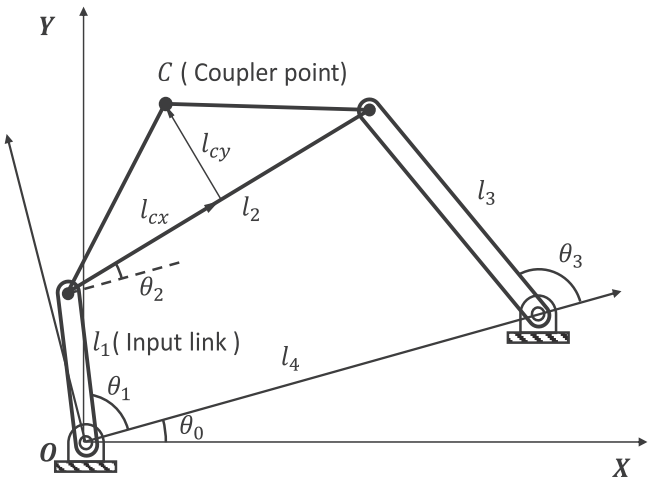

Fig. 1. Four-bar Linkage mechanism in a global coordinate system.

$$T_3 = l_3 + l_2 - l_1 - l_4 > 0 \tag{1c}$$

Each variable can be found in Fig. 1. If the input link (l_1) rotates once, a coupler curve is generated that is the same as the trajectory of the coupler point of the four-bar linkage. Fig. 1 shows the position of coupler point C on a four-bar linkage, which is described as follows:

$$C_x = l_1 \cos(\theta_1 + \theta_0) + l_{cx} \cos(\theta_2 + \theta_0) - l_{cy} \sin(\theta_2 + \theta_0) \tag{2a}$$

$$C_y = l_1 \sin(\theta_1 + \theta_0) + l_{cx} \sin(\theta_2 + \theta_0) + l_{cy} \cos(\theta_2 + \theta_0) \tag{2b}$$

Because the four-bar linkage has one degree of freedom, the angle θ_2 can be represented by the input angle θ_1. Freudestein's equation was used to determine the relationship between θ_2 and the input angle [18]:

$$K_1 \cos\theta_3 - K_2 \cos\theta_1 + K_3 = \cos(\theta_1 - \theta_3) \tag{3a}$$

$$K_1 \cos\theta_2 - K_4 \cos\theta_1 + K_5 = \cos(\theta_1 - \theta_2) \tag{3b}$$

where

$$K_1 = \frac{l_4}{l_1}, K_2 = \frac{l_4}{l_3}, K_3 = \frac{{l_1}^2 - {l_2}^2 + {l_3}^2 + {l_4}^2}{2 l_1 l_3}, K_4 = \frac{l_4}{l_2}, K_5 = \frac{{l_3}^2 - {l_4}^2 - {l_1}^2 - {l_2}^2}{2 l_1 l_2}.$$

From Eqs. (3a) and (3b), the solutions of θ_2 and θ_3 regarding the input angle θ_1 are obtained as follows:

$$\theta_2 = 2 \tan^{-1}\left\{\left(-B \pm \sqrt{B^2 - 4AC}\right)/2A\right\} \tag{4a}$$

$$\theta_3 = 2 \tan^{-1}\left\{\left(-E \pm \sqrt{E^2 - 4EF}\right)/2D\right\} \tag{4b}$$

where

$$A = \cos\theta_1 - K_1 + K_4 \cos\theta_1 + K_5$$

$$B = -2 \sin\theta_1$$

$$C = K_1 + (K_4 - 1)\cos\theta_1 + K_5$$

$$D = \cos\theta_1 - K_1 + K_2 \cos\theta_1 + K_3$$

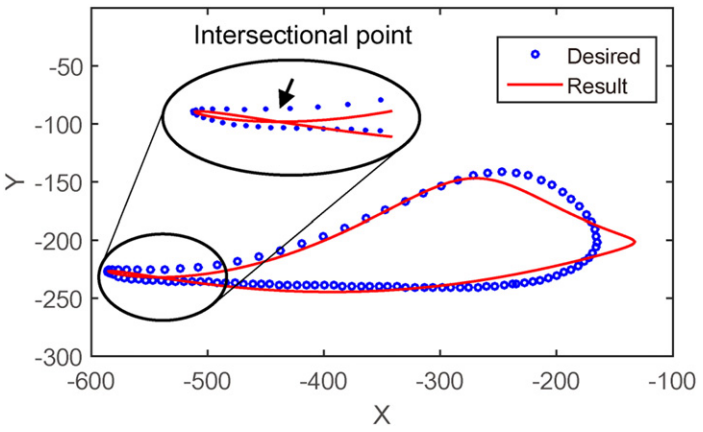

Fig. 2. The result of a case study for determining a four-bar linkage that can trace a human gait trajectory obtained by motion capture.

$$E = -2\sin\theta_1$$

$$F = K_1 - (K_2 + 1)\cos\theta_1 + K_3$$

Substituting Eq. (4a) into Eqs. (2a) and (2b) allows for the derivation of the coupler point position of a four-bar linkage using a single variable in the range of [0 2π].

2.2. Classification of shape of trajectories

2.2.1. Motivation: unintended shape

When designing a four-bar linkage that can trace a target trajectory by minimizing TE, unintended shapes of the coupler curve can sometimes be obtained, as shown in Fig. 2. To avoid this, the coupler curves were classified into specific types of shapes and used to design a mechanism. For example, the solution for the desired trajectory demonstrated in Fig. 2, which is part of the "non-intersectional shape" category, would not normally be obtained.

2.2.2. Classification methodology

The four shape categories are shown in Fig. 3. The ellipse-like shape is Type-I, the shape that includes linear motions is Type-II, the crescent-like shape is Type-III, and the shape that has an intersection point is Type-IV. Two methods were used to validate this classification. The first method is visual inspection of the coupler curves of the atlas by Hrones and Nelson [1]. Approximately 7000 coupler curves were categorized. This method does not need further work such as coding, so it is easy and simple to apply this method to the atlas. However, because visual inspection is done with the human eye, the accuracy and reproducibility of the result may low.

The second method is generating link lengths of a four-bar linkage randomly and checking whether or not each trajectory belongs to one of the four types using the geometrical characteristics of each type. Over 100,000 coupler curves were examined. Since the shape is the only thing to be considered in the classification, the generated trajectories were rotated to have the maximum width, as shown in Fig. 4. We found a vector which has maximum length in the trajectory, and rotated the trajectory by the slope of the vector relative to the origin point. After rotating the trajectory, the geometrical characteristics were considered. The details are described in the next section. Once the geometrical features are coded for a computer simulation, it is easy to classify a large number of coupler curves. The simulation also enables very high accuracy and reproducibility of the results compared to visual inspection. However, the geometrical characteristics are needed, and programing takes more time.

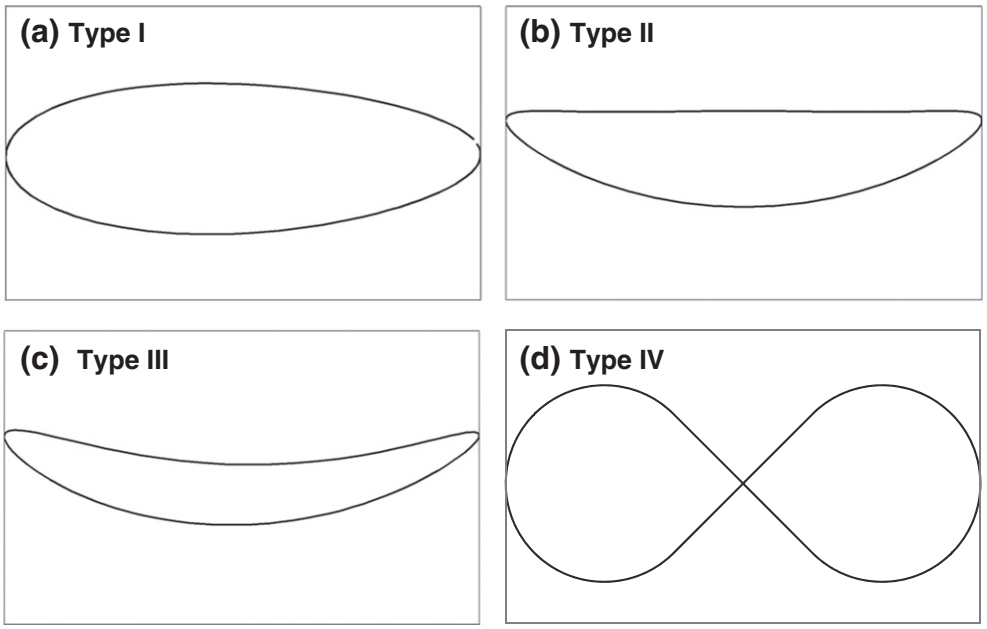

Fig. 3. Categories of the trajectories of crank-rocker four-bar linkage: (a) Type-I (ellipse shape), (b) Type-II (semi-ellipse shape), (c) Type-III (crescent-like shape), (d) Type-IV (Intersectional shape).

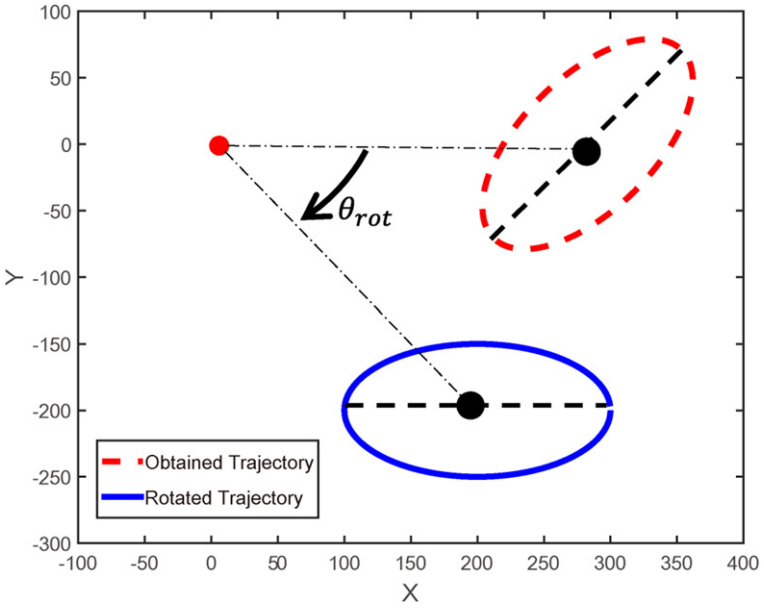

Fig. 4. To facilitate the distinguishing of shapes, the obtained trajectory was rotated by $\boldsymbol{\theta_{rot}}$ to have the maximum width.

2.2.3. Geometrical characteristics of each type of trajectory

The geometrical characteristics that distinguish each shape type are the first-order and second-order derivatives of the coupler curve of a four-bar linkage and the radius of curvature of some sections of the trajectory. These characteristics are described as follows:

First-order derivative (slope):

$$\frac{\partial C_y}{\partial C_x} = \frac{\partial C_y}{\partial \theta_1}\frac{\partial \theta_1}{\partial C_x} \tag{5a}$$

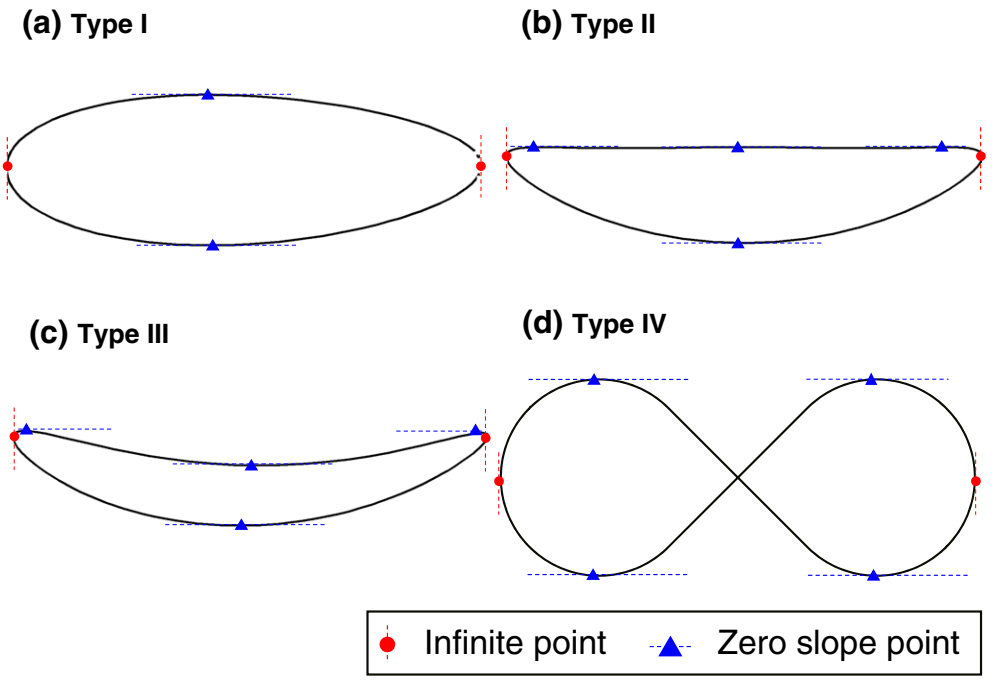

Fig. 5. Infinite points and zero-slope point of trajectories.

Second-order derivative (change in angle of slope):

$$\frac{\partial^2 C_y}{\partial {C_x}^2} = \frac{\partial}{\partial C_x}\left(\frac{\partial C_y}{\partial C_x}\right) = \left(\frac{\partial C_x}{\partial \theta_1}\frac{\partial^2 C_y}{\partial {\theta_1}^2} - \frac{\partial^2 C_x}{\partial {\theta_1}^2}\frac{\partial C_y}{\partial \theta_1}\right) \Big/ \left(\frac{\partial C_x}{\partial \theta_1}\right)^3 \tag{5b}$$

Radius of curvature:

$$R = \left| \left(1 + \frac{\partial {C_x}^2}{\partial C_y}\right)^{\frac{3}{2}} \Big/ \frac{\partial^2 C_x}{\partial {C_y}^2} \right| \tag{5c}$$

If the derivative values are plotted according to the input angle θ_1, there are only two points at which the first-order derivative is infinite for all types. The infinite points divide the trajectory into an upper side and lower side, as demonstrated in Fig. 5. In the case of Type-I, there is one zero-slope point for each part, where the first-order derivative is zero. In addition, the sign of the second-order derivative at the zero-slope points is different for each side of the trajectory. The sign of the upper zero-slope point is negative, and that of the lower side is positive.

In Type-II, there are one or three points on the flat side and one on the other side. Since the flat side does not include a straight line, the number of zero-slope points varies from one to three. Thus, the radius of curvature is used to distinguish this type from the others. If the radius of curvature of one side is almost infinite, the shape must be classified as Type-II.

In the case of Type-III, there are three zero-slope points on one side and one on the other side. In addition, the signs of the second-order derivative of each side are the same. Finally, in Type-IV, there are two zero-slope points per side. Table 1 gives a summary of these geometrical features.

2.2.4. Classification results and discussion

Using the method described in the previous section, 6889 coupler curves were examined, and the results are shown in Table 2. Among the coupler curves of the atlas, Type-I elliptical shapes account for 59.22% of the total coupler curves. Types-II, III, and IV account for 10.77%, 21.55%, and 8.36%, respectively. 0.1% of all coupler curves cannot be categorized into one of the four types. In particular, two of them had an elliptical shape, but there were five zero-slope points on one side. Another one had an intersectional shape, but the number of zero-slop points was the same as Type III. Thus, these exceptional samples have two intersectional points.

Similar results can be observed with the second methodology. A total of 10,165 coupler curves were examined using the second method. Among all trajectories of randomly generated four-bar linkages, Type-I accounts for 66.47%, while Types- II, III, and IV account for 5.90%, 19.69%, and 7.91%, respectively. In this case, there are only three exceptions. One is the same as the latter exception of the first method. Another case has four infinite points, and the third one has an intersectional shape, but it has four zero-slope points on one side of the trajectory.

Because of the difference in the boundaries of each link length, it seems that the results of each method are slightly different. But each result shows the same trends. Despite the exceptional trajectory shapes, the results show that four shape types can cover 99.95% of all of the trajectories. The 10 exceptional cases are not enough to be considered as a single category, so they were assumed to be negligible.

The classification in this paper has two advantages compared to exist classification [19]. First, because four categories are easy to distinguish from each other, a designer can easily choose a category that involves the shape of desired trajectory by visual inspection. Second, the geometrical properties used for the classification are simple to calculate. This means that the classification process in computer simulation is so fast that if this classification is used for the design of four-bar linkage, whole design time can be reduced.

3. New approach for four-bar linkage design

The first and second-order derivatives of the coupler points include the geometrical features used to distinguish the coupler curves, which we prove in this section. Furthermore, the new methodology based on these features is presented.

Table 1
Geometrical properties of each shape type.

Type		I	II	III	IV
Num. of Infinite points		2	2	2	2
Zero-slope point ratio		1:1	1:1 or 1:3	1:3	2:2
Sign of second derivative at zero slope point	Upper	-	- or +	+	+/-
	Lower	+	+	+	-/+
Radius of curvature		Finite	Infinite	Finite	Finite

Table 2
Classification results with methods 1 & 2.

	First method (visual inspection)	Second method (using geometrical features)
Type I	4081 (0.5922)	6757 (0.6647)
Type II	742 (0.1077)	600 (0.0590)
Type III	1485 (0.2155)	2001 (0.1969)
Type IV	574 (0.0836)	804 (0.0791)
Exception	7 (0.0010)	3 (0.0003)
Total	6889 (1.0000)	10,165 (1.0000)

3.1. Geometrical meaning of first-order derivative (slope) of coupler point

The slope is frequently used to distinguish coupler curves. Based on this, we propose the following geometrical interpretation of the first-order derivative of the coupler point:

Proposition 1. If two plane figures have the same first-order derivative profile, they can be called mathematically similar.

Proof of Proposition 1. *In the discrete system and based on Fig. 6,*

(1) $i = 1$

If $\varphi_{1,1} = \varphi_{2,1}$, then Δ O $p_{1,1}$ $p_{1,2}$ and Δ O $p_{2,1}$ $p_{2,2}$ are similar. The similarity ratio is $\frac{n_1 r_1}{r_1} = n_1$.

The tangent values of angles $\varphi_{1,1}$ and $\varphi_{2,1}$ are described as follows:

$$\tan\varphi_{1,1} = \frac{\Delta y}{\Delta x} = \frac{r_2 \sin\xi_2 - r_1 \sin\xi_1}{r_2 \cos\xi_2 - r_1 \cos\xi_1} \tag{6a}$$

$$\tan\varphi_{2,1} = \frac{n_2 r_2 \sin\xi_2 - n_1 r_1 \sin\xi_1}{n_2 r_2 \cos\xi_2 - n_1 r_1 \cos\xi_1} \tag{6b}$$

Because $\varphi_{1,1}$ and $\varphi_{2,1}$ are assumed to be the same, Eqs. (6a) and (6b) are the same. This implies that the similarity ratios n_1 and n_2 are the same.

(2) $i = k$

If $\varphi_{1,k} = \varphi_{2,k}$, then Δ O $p_{1,k}$ $p_{1,k+1}$ and Δ O $p_{2,k}$ $p_{2,k+1}$ are similar. The similarity ratio is $\frac{n_k r_k}{r_k} = n_k$.

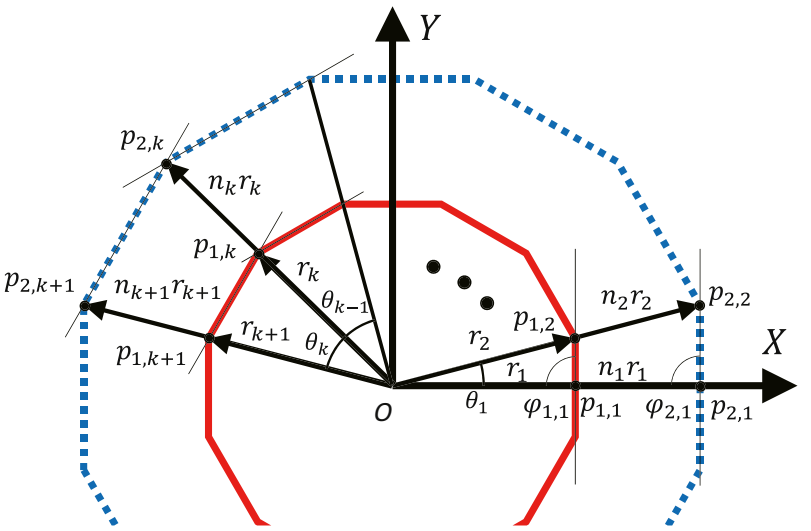

Fig. 6. Diagram for the proof of Proposition 1.

The tangent values of angles $\varphi_{1,k}$ and $\varphi_{2,k}$ are described as follows:

$$tan\,\varphi_{1,k} = \frac{\Delta y}{\Delta x} = \frac{r_{k+1}\,sin\,\xi_{k+1} - r_k\,sin\,\xi_k}{r_{k+1}\,cos\,\xi_{k+1} - r_k\,cos\,\xi_k} \tag{7a}$$

$$tan\,\varphi_{2,k} = \frac{n_{k+1}r_{k+1}\,sin\,\xi_{k+1} - n_k r_k\,sin\,\xi_k}{n_{k+1}r_{k+1}\,cos\,\xi_{k+1} - n_k r_k\,cos\xi_k} \tag{7b}$$

Because $\varphi_{1,k}$ and $\varphi_{2,k}$ are assumed to be the same, Eqs. (7a) and (7b) are the same. This implies that the similarity ratios n_k and n_{k+1} are the same.

By mathematical induction, the similarity ratio of step k (n_k) is the same as that of step 1 (n_1). This means that if two plane figures have the same first-order derivative in all discrete segments, they are mathematically similar. This can also be applied to a continuous system by decreasing the interval angle ξ_k.

3.2. Geometrical meaning of second-order derivative (change in angle of slope) of coupler point

In the previous section, the sign of the second-order derivative was also used to distinguish the coupler points. Thus, we propose the following geometrical interpretation of the derivative:

Proposition 2. If two plane figures have the same first and second-order derivative profiles, they are the same figure.

Proof Of Proposition 2. *The second-order derivative value can be obtained as follows*:

$$\frac{\partial^2 C_y}{\partial {C_x}^2}_{small} \sim \frac{\Delta\left(\Delta y / \Delta x\right)}{\Delta x} = \frac{tan^{-1}\varphi_{1,k+1} - tan^{-1}\varphi_{1,k}}{r_k\left(cos\xi_{sum(k)} - cos\xi_{sum(k-1)}\right)} \tag{8a}$$

$$\frac{\partial^2 C_y}{\partial {C_x}^2}_{big} \sim \frac{\Delta\left(\Delta y / \Delta x\right)}{\Delta x} = \frac{tan^{-1}\varphi_{1,k+1} - tan^{-1}\varphi_{1,k}}{n_k r_k\left(cos\xi_{sum(k)} - cos\xi_{sum(k-1)}\right)} \tag{8b}$$

where

$$\xi_{sum(k)} = \sum_{i=1}^{k} \xi_i$$

If the second-order derivative values of each plane figure are the same, Eq. (8a) is equal to Eq. (8b).

$$\frac{\partial^2 C_y}{\partial {C_x}^2}_{big} = \frac{1}{n_k}\frac{\partial^2 C_y}{\partial {C_x}^2}_{small} \tag{9}$$

Eq. (9) shows that the similarity ratio n_k has to be one. In other words, the two plane figures are exactly the same.

3.3. New approach for four-bar linkage design

To obtain an optimal trajectory numerically without the possibility of generating an unintended trajectory shape, the following two-step optimization problem was developed:

First step of optimization:

$$\min_{X_{link} \in R^5} RMS(1st\ deriv._G - 1st\ deriv._D)$$

Subject to: Desired shape (distinguished by geometrical features).
$T_1, T_2, T_3 > 0$ (Grashof condition).

Second step of optimization:

$$\min_{X_{size} \in R} RMS(2nd\ deriv._G - 2nd\ deriv._D)$$

Subject to: $X_{link} = X_{link}^{*}$.
where:
$RMS(x)$: Root mean square value of x
$n\ th\ derive._G$: $n\ th$-order derivative equation of generated trajectory
$n\ th\ derive._D$: $n\ th$-order derivative equation of desired trajectory

$$X_{link} = [\, l_2 \quad l_3 \quad l_4 \quad l_{cx} \quad l_{cy} \,]/l_1$$

X_{link}^{*}: Optimal value of first step of optimization

$$X_{size} = l_1$$

Because of Proposition 1, the shape of the trajectory is determined in the first step, in which the RMS value of the first-order derivative error between the generated trajectory and target is minimized. After that, due to Proposition 2, the size of the trajectory is determined by the second step of optimization, in which the RMS value of the second-order derivative error between the generated trajectory and target is minimized. The reason for dividing the optimization process into two steps is that the design variables can be separated into two groups: shape-dependent and size dependent variables. The shape-dependent variable is X_{link}, which contains the rations of the link lengths to l_1. The only size-dependent variable is l_1, which is the standard of X_{link}.

3.4. Optimization algorithm: hybrid Taguchi-random coordinate search algorithm

To find the optimal value of each step, an optimization algorithm is required. The objective function used in this paper is composed of an obvious equation, but it is too complex to analyze the function analytically. This type of function is treated as a black-box function [20]. To optimize the black-box function, derivative-free optimization (DFO) algorithms such as genetic algorithms (GA), simulated annealing (SA), or pattern search optimization (PSO) are applied [21]. However, these methodologies are limited in that they sometimes cannot find global optimal points. Rios and Sahinidis [21] suggest that a better solution to this kind of problem may be a combination of two algorithms. Thus, the hybrid Taguchi-random coordinate search algorithm (HTRCA) is applied [22]. HTRCA combines the Taguchi method (TM) with the random coordinate search algorithm (RCA) to find the optimal solution of the objective functions.

4. Case studies

This section analyzes a number of cases that were investigated with the developed algorithm to validate the method. For a performance comparison, the conventional method that minimizes tracking error is used. The input data set of the given points and their intervals is controlled for unprejudiced comparison. The method minimizes the tracking error of the given data set and finds the optimal mechanism. Moreover, the method developed in this paper derives the optimal mechanism to minimize the objective function with the reference slope and its change in angle of slope, which are estimated from the given data set.

4.1. Case 1–1: type-I (equal intervals)

The desired trajectory of the first case is a mathematical ellipse described as follows:

$$\frac{(x - x_0)^2}{a^2} + \frac{(y - y_0)^2}{b^2} = 1 \tag{10}$$

1000 coupler points were chosen to identify the optimal solution that can trace an ellipse with a = 100 and b = 50. Because the purpose of this case study is to find the shape and size of the trajectory, the position variables x_0 and y_0 are not needed. Therefore, for this problem,
Target curve:

$$C_{x,D} = 100 \cos\theta \tag{11}$$

$$C_{y,D} = 50 \sin\theta \tag{12}$$

$$\theta = \mathrm{i}/1000, \mathrm{i} = 1, \ldots, 1000$$

Constraint conditions:
Desired shape: Type-I

$$X_{size} \in (0, 500]$$

$$[l_2 \quad l_3 \quad l_4]/l_1 \in (0, 10]$$

$$[l_{cx} \quad l_{cy}]/l_1 \in [-10, 10]$$

4.2. Case 1–2: type-I (variable intervals)

This case is also an ellipse described by Eq. (10). In some real situations, the velocity of each section needs to be considered. Therefore, the velocity profile of the coupler points is modified from the first case. The other conditions are the same. For this problem,

Target curve:

$$C_{x,D} = \begin{cases} 100\cos\left(\frac{i}{550}\pi\right) & i = 1, \ldots, 550 \\ 100\cos\left(\pi + \frac{i-550}{450}\pi\right) & i = 551, \ldots, 1000 \end{cases} \tag{13}$$

$$C_{y,D} = \begin{cases} 50\sin\left(\frac{i}{550}\pi\right) & i = 1, \ldots, 550 \\ 50\sin\left(\pi + \frac{i-550}{450}\pi\right) & i = 551, \ldots, 1000 \end{cases} \tag{14}$$

Constraint conditions:
Desired shape: Type-I

$$X_{size} \in (0, 500]$$

$$[l_2 \quad l_3 \quad l_4]/l_1 \in (0, 10]$$

$$[l_{cx} \quad l_{cy}]/l_1 \in [-10, 10]$$

4.3. Case 2–1: type-III (equal interval)

The desired trajectory of case 2 looks like a crescent, as shown in Fig. 7 (A). The desired velocity in all sectors is constant. For this problem, the target curve and constraint conditions are as follows.

Target curve:
The value of parameter composing the shape of the desired trajectory is demonstrated in Fig. 7(A).
1000 coupler points in total are positioned equidistantly.
Constraint conditions:
Desired shape: Type-III

$$X_{size} \in (0, 100]$$

$$[l_2 \quad l_3 \quad l_4]/l_1 \in (0, 10]$$

$$[l_{cx} \quad l_{cy}]/l_1 \in [-10, 10]$$

The distance between centerline and input point is smaller than 20.

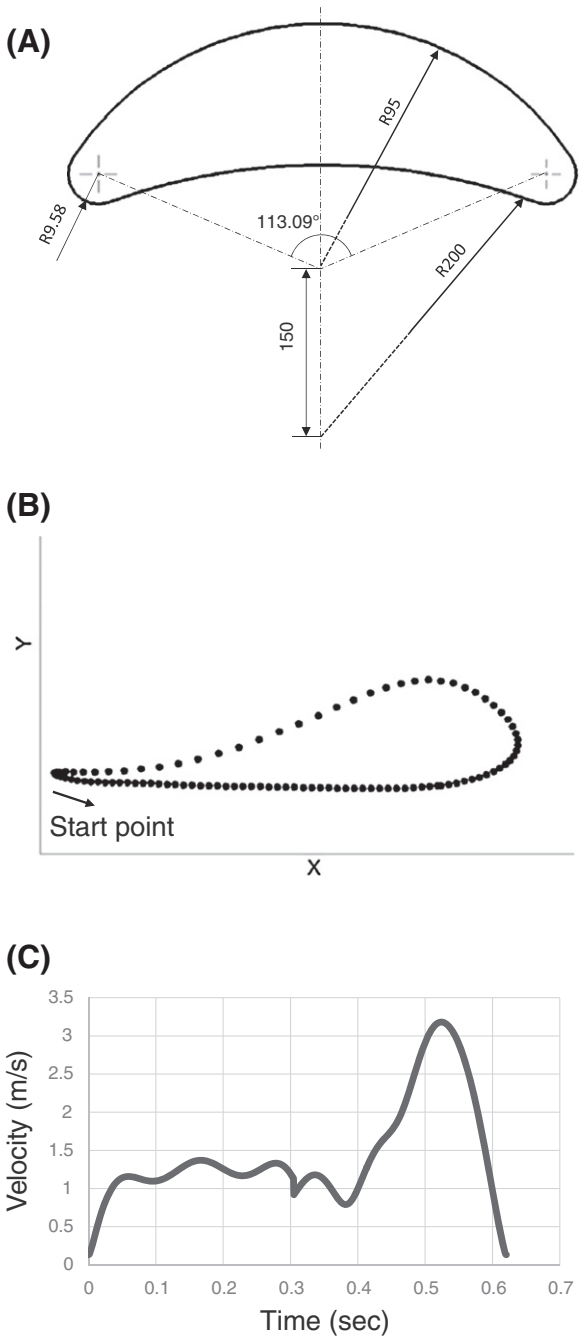

Fig. 7. Desired trajectories of case study (A) Case 2 (B) Case 3.

4.4. Case 2–2: type-III (variable intervals)

The shape of the trajectory in this case is the same as case 2–1, except for the desired velocity of each section. Instead of constant velocity, the velocity of the lower side of the trajectory is 10% slower than that of the previous case with the same constraints. Therefore, for this problem, the target curve and constraint conditions are as follows.

Target curve:
The shape of the trajectory is the same as case 2–1
The interval between each points of the upper side is 10% larger than that of case 2–1.
The interval between each point of the lower side is 10% smaller than that of case 2–1.

Constraint conditions:
Desired shape: Type-III

$$X_{size} \in (0, 100]$$

$$[l_2 \quad l_3 \quad l_4]/l_1 \in (0, 10]$$

$$[l_{cx} \quad l_{cy}]/l_1 \in [-10, 10]$$

The distance between the centerline and input point is less than 20.

4.5. Case 3: avoiding intersectional shapes

This case is from a real application of generating a human gait trajectory for the rehabilitation of a person who has difficulties in walking. The human gait trajectory was captured by a motion capture system, and 101 coupler points were composed, as illustrated in Fig. 7 (B). For this problem, the target curve and constraint conditions are as follows. In this case, the target curve is not equation like previous cases. So we estimate target points to sine and cosine curve, and a slope and angle of slope profile are calculated using derivation of estimated curve.

Target curve:
The trajectory shape is depicted in Fig. 7(B).
101 points captured by motion capture system.
Constraint conditions:
Desired shape: Type-I, II, and III

$$X_{size} \in (0, 200]$$

$$[l_2 \quad l_3 \quad l_4]/l_1 \in (0, 10]$$

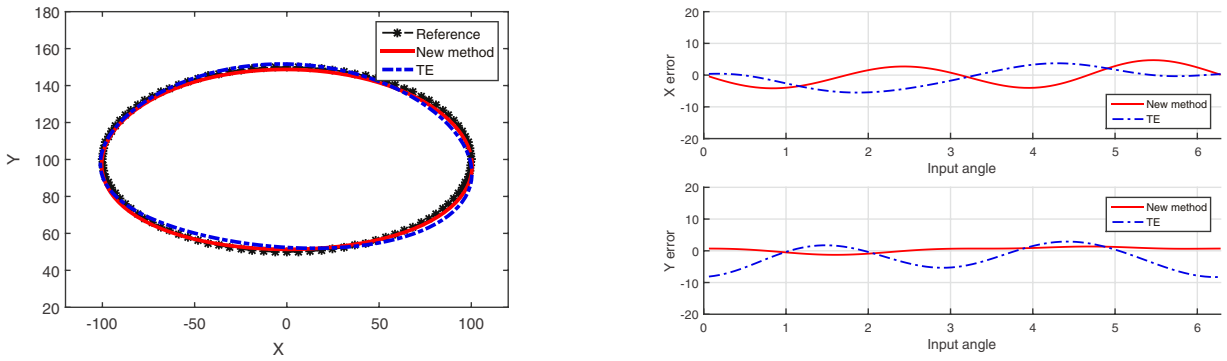

< Simulation Result of Case 1-1 (Left) Trajectory of coupler point (Right upper) X error V.S. input angle (Right lower) Y error V.S. input angle >

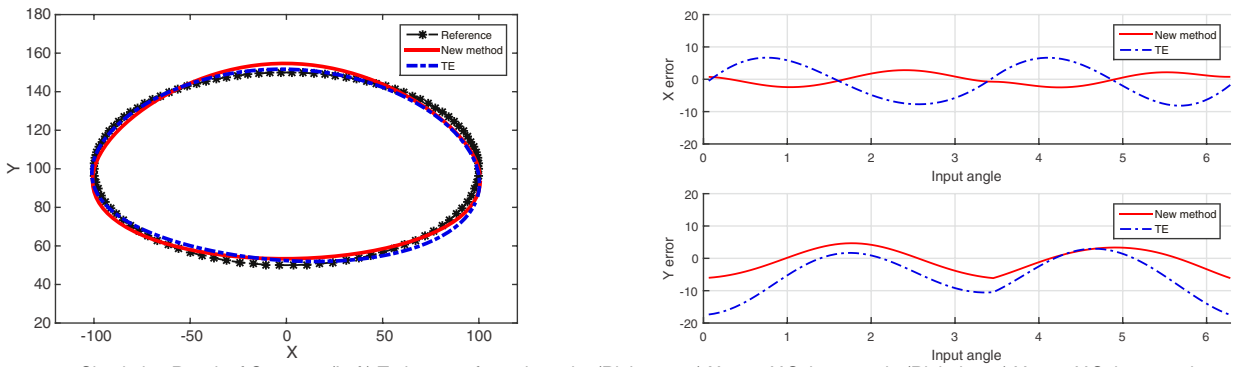

< Simulation Result of Case 1-2 (Left) Trajectory of coupler point (Right upper) X error V.S. input angle (Right lower) Y error V.S. input angle >

Fig. 8. Simulation result of case 1 (ellipse shape).

$$[l_{cx} \quad l_{cy}]/l_1 \in [-10, 10]$$

5. Comparative results and discussion

5.1. Goodness of traceability index for objective comparison

To compare the performance of each method, an index for objective comparison is necessary. If the value of the developed objective function is used for comparing the performance, the new method minimizes that value and will naturally show better performance than other methods. There are various indexes that evaluate the performance of a design methodology. The most common index is tracking error, as mentioned. Because only the distance between the generated trajectory and target is calculated, TE cannot represent the velocity of the coupler point. Other indexes such as mismatch area error [23] and structure error [24] also cannot represent the velocity of the coupler point. Therefore, we defined the GT index, which can represent the shape and velocity simultaneously for objective comparison. GT is defined as the tracking error according to the input angle. To calculate the GT, the x and y error, that difference between desired value and obtained trajectory, are plotted according to input angle shown in the right side of the Figs. 8, 9 and 10. Then, root-mean-square value of x and y error is calculated which is same as GT.

5.2. Discussion

The case study results are shown in Table 3. Fig. 8 shows the obtained trajectory and the position of the coupler point according to the input angle of case 1–1 and case 1–2. The trajectory shapes obtained by the TE-minimizing method are the same in cases 1–1 and 1–2. In contrast, the shapes obtained by the new method are different for these cases. These results show that the new approach can take account of the velocity profile of each section of the trajectory, in contrast to the conventional TE approach. There are two peaks in the reference. If the results do not follow these peaks, RMSEs of first and second order derivative are very large. Thus, to minimize the objective function, the peaks of slope and the change in angle of slope of the generated mechanism have to match with the reference naturally. It implies that the time portion of each section (upper and lower) of the generated mechanism is the same as that of the reference. This is the reason that the new method can take account of the velocity of each section of the trajectory.

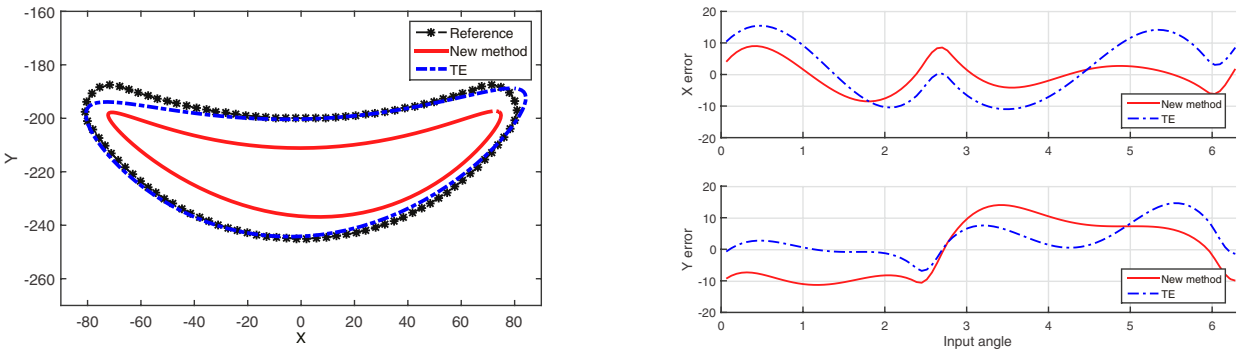

< Simulation Result of Case 2-1 (Left) Trajectory of coupler point (Right upper) X error V.S. input angle (Right lower) Y error V.S. input angle >

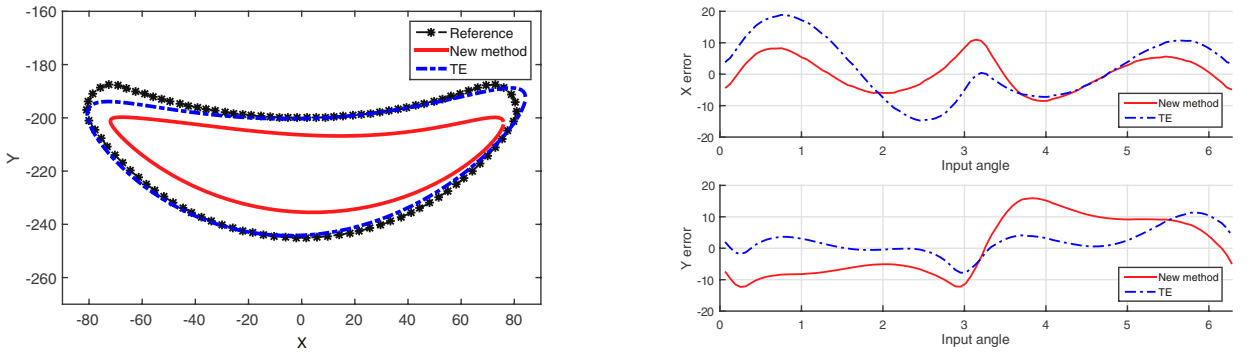

< Simulation Result of Case 2-2 (Left) Trajectory of coupler point (Right upper) X error V.S. input angle (Right lower) Y error V.S. input angle >

Fig. 9. Simulation result of case 2 (crescent-like shape).

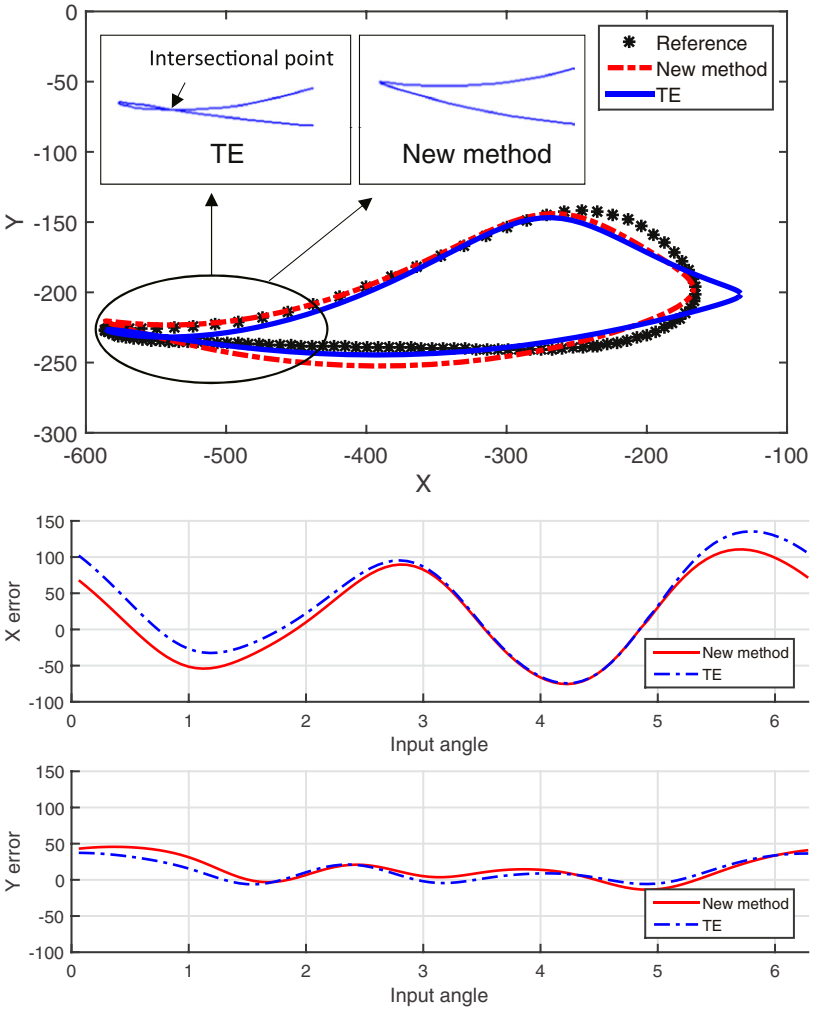

Fig. 10. Simulation result of case 3 (walking motion).

The GT values show this advantage very well. The GT values of the new method are smaller than those of the conventional method in both cases 1–1 and 1–2. This indicates that the new method can take account of the trajectory shape and velocity simultaneously.

The results of case 2 are shown in Fig. 9. Considering only the trajectory shape, the performance of the new approach is poorer than that of the conventional method. However, the GT of the new approach is lower than that of the method that minimizes TE. Despite the conventional trajectory looking similar to the desired trajectory, the error of the x value according to the input angle is larger than that of the result from the new method, as shown on the right side of Fig. 9. This result also shows the velocity consideration of the new approach.

Table 3
Comparative results of case studies.

	Case 1–1		Case 1–2		Case 2–1		Case 2–2		Case 3	
	New	TE	New	TE	New	TE	New	TE	New	TE
l_1	68.37	50.50	81.12	50.50	13.6	22.13	14.5016	22.13	184.00	193.60
l_2	417.03	157.81	494.84	157.81	29.24	48.12	24.64754	48.12	336.60	344.80
l_3	403.35	282.80	527.28	282.80	76.84	206.87	40.59855	206.87	346.60	378.20
l_4	676.81	361.08	766.59	361.08	89.76	219.59	50.02718	219.59	464.27	509.27
l_{cx}	88.88	−118.68	811.21	−118.68	136	212.40	−92.7999	212.40	404.41	382.21
l_{cy}	−252.95	−90	381.26	−90	−102	65.2687	−18.8499	65.2687	155.08	205.88
θ_0	−0.3253	3.2987	2.6755	3.2987	0.0135	3.2515	0.4749	3.2515	2.5483	2.4428
GT	2.0896	3.5437	2.7146	6.8365	7.2603	7.8451	7.5514	7.5989	46.3896	51.4451

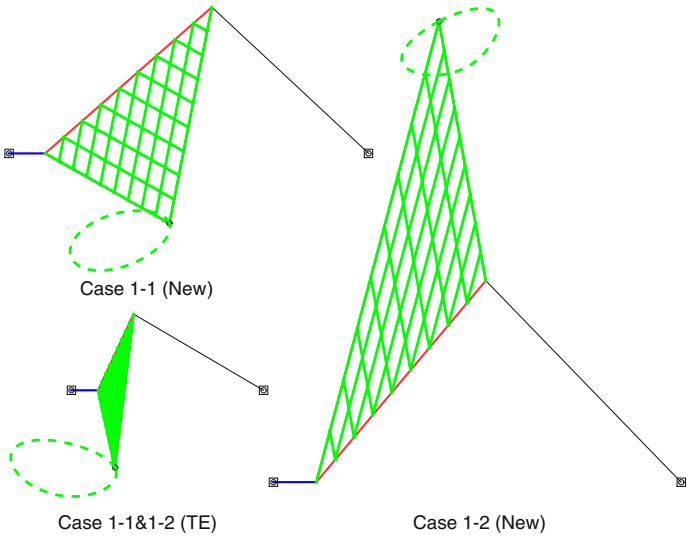

Fig. 11. Four-bar linkage mechanism of case study 1(Input link: blue link, not rotated).

The results of case study 3 are depicted in Fig. 10. The intersectional shape of the trajectory is obtained by the TE-minimizing method. The purpose of this problem is a rehabilitation application. With the conventional method, a four-bar linkage that makes an intersectional trajectory shape cannot be the solution. The trajectory shape obtained by the new approach does not have an intersectional point, which satisfies the requirements, as shown in Fig. 10. The GT of the new approach is also smaller than that of the conventional method. The four-bar linkage mechanisms from the result of case studies are demonstrated in Figs. 11, 12 and 13.

The proposed design method is more reliable than the TE-based method, because there is no possibility of generating unintended shapes. In addition, the method includes the velocity profile, which allows the design method to obtain trajectories with various velocities.

Practical application of the proposed method is very important to prove the reliability of the method. Angular transmission device is one of very suitable example to emphasize the functionality of the method that the device requires high speed operation with different velocity path. You can refer the conference paper of the authors to see the application results of the proposed method to the angular transmission device [25].

6. Conclusion

The trajectories of a crank-rocker four-bar linkage were grouped into four types, and a new approach was presented based on the classification. The approach involved one step for minimizing the RMSE of the first-order derivative to obtain a similar

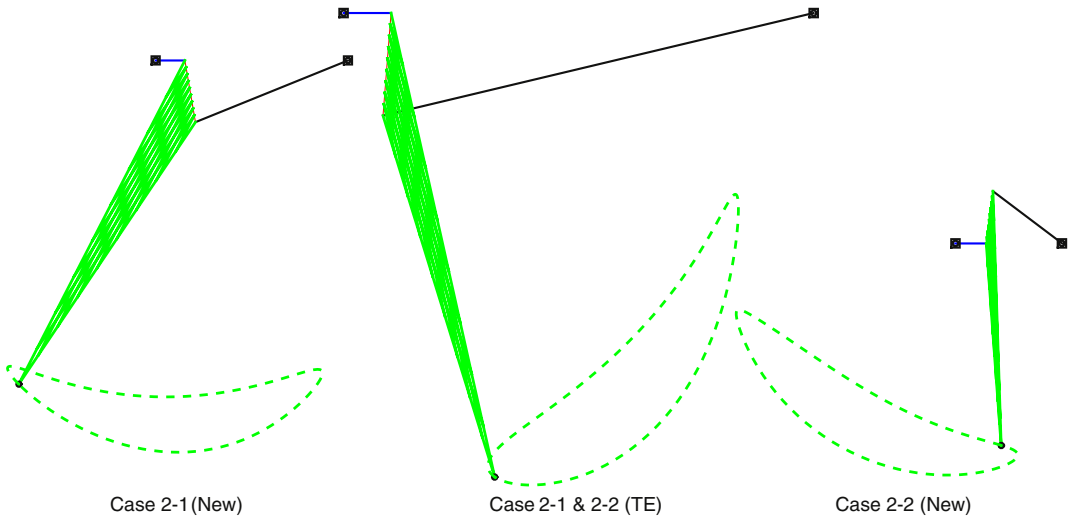

Fig. 12. Four-bar linkage mechanism of case study 2(Input link: blue link, not rotated).

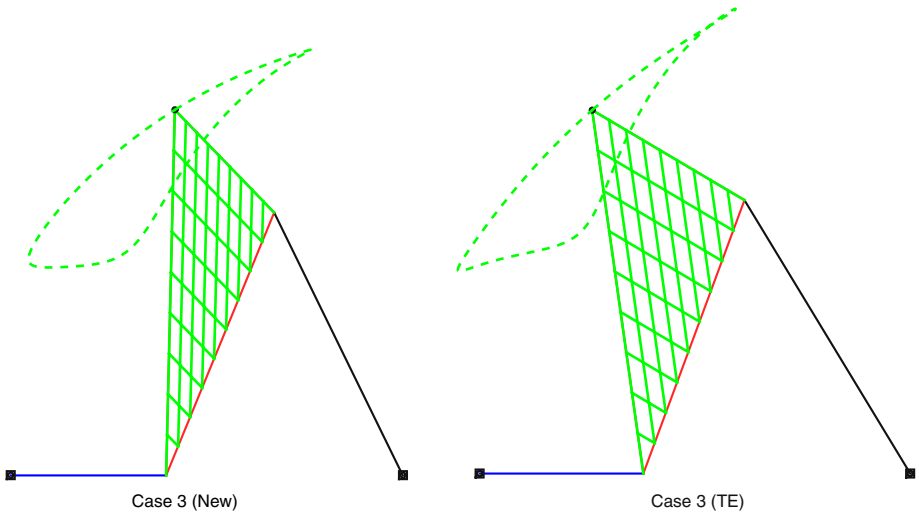

Fig. 13. Four-bar linkage mechanism of case study 3(Input link: blue link, not rotated).

trajectory shape to the target trajectory, and a second step to obtain an optimal shape that can trace the target trajectory by minimizing the RMSE of the second-order derivative.

The proposed method has three advantages over the conventional method: the reference can be set to a continuous function, the method can take account of the velocity of each side of the trajectory, and it can avoid obtaining unintended trajectories based on the geometrical features. To compare the performance of the new approach objectively, the GT index was defined to take account of the shape and velocity of the trajectory simultaneously. The GT values showed the advantages of the new approach in case studies.

However, this methodology has some limitations. First, the target mechanism was limited to a crank-rocker four-bar linkage. Second, further work is needed to apply this new method to non-continuous target trajectories, such as in case 3. Future studies will be conducted to overcome these limitations. The practical applications will also be examined in the next study.

Acknowledgment

This study was supported by the Basic Science Research Program through the National Research Foundation of Korea (NRF)funded by the Ministry of Education (NRF-2014R1A1A4A01009290).

References

[1] J.A. Hrones, Analysis of the Four-Bar Linkage, Published Jointly by the technology Press of the Massachusetts Institute of Technology, and Wiley, 1951.
[2] Sandor, G. N., A general complex-number method for plane kinematic synthesis with applications (Doctoral dissertation, Columbia University.), 1959.
[3] C.Y. Han, A general method for the optimum design of mechanisms, J. Mech. 1 (3) (1967) 301–313.
[4] R. Sancibrian, F. Viadero, P. Garcıa, A. Fernández, Gradient-based optimization of path synthesis problems in planar mechanisms, Mech. Mach. Theory 39 (8) (2004) 839–856.
[5] W.Y. Lin, A GA–DE hybrid evolutionary algorithm for path synthesis of four-bar linkage, Mech. Mach. Theory 45 (8) (2010) 1096–1107.
[6] R. Zbikowski, C. Galinski, C.B. Pedersen, Four-bar linkage mechanism for insectlike flapping wings in hover: concept and an outline of its realization, J. Mech. Des. 127 (4) (2005) 817–824.
[7] J.S. Zhao, Z.F. Yan, L. Ye, Design of planar four-bar linkage with n specified positions for a flapping wing robot, Mech. Mach. Theory 82 (2014) 33–55.
[8] C. Zhang, R.L. Norton, P.E ., T. Hammonds, Optimization of parameters for specified path generation using an atlas of coupler curves of geared five-bar linkages, Mech. Mach. Theory 19 (6) (1984) 459–466.
[9] A.G. Erdman, G.N. Sandor, S. Kota, Mechanism Design: Analysis and Synthesis (Vol. 1), Prentice-Hall, Englewood Cliffs, 1984.
[10] A.G. Erdman, Three and four precision point kinematic synthesis of planar linkages, Mech. Mach. Theory 16 (3) (1981) 227–245.
[11] C.W. Wampler, A.P. Morgan, A.J. Sommese, Complete solution of the nine-point path synthesis problem for four-bar linkages, J. Mech. Des. 114 (1) (1992) 153–159.
[12] J. Chu, W. Cao, Synthesis of coupler curves of planar four-bar linkages through fast fourier transform, Chin. J. Mech. Eng. 29 (5) (1993) 117–122.
[13] J.R. McGarya, Rapid search and selection of path generating mechanisms from a library, Mech. Mach. Theory 29 (2) (1994) 223–235.
[14] I. Ullah, S. Kota, Optimal synthesis of mechanisms for path generation using Fourier descriptors and global search methods, J. Mech. Des. 119 (4) (1997) 504–510.
[15] S. Krishnamurty, D.A. Turcic, Optimal synthesis of mechanisms using nonlinear goal programming techniques, Mech. Mach. Theory 27 (5) (1992) 599–612.
[16] J.A. Cabrera, A. Simon, M. Prado, Optimal synthesis of mechanisms with genetic algorithms, Mech. Mach. Theory 37 (10) (2002) 1165–1177.
[17] J.M. McCarthy, G.S. Soh, Geometric Design of Linkages, 11Springer, 2010.
[18] F. Freudenstein, Design Of Four-Link MechanismsPh. D. Thesis Columbia University, USA, 1954.
[19] D.A. Hoeltzel, W.H. Chieng, Pattern matching synthesis as an automated approach to mechanism design, J. Mech. Des. 112 (2) (1990) 190–199.
[20] D.R. Jones, M. Schonlau, W.J. Welch, Efficient global optimization of expensive black-box functions, J. Glob. Optim. 13 (4) (1998) 455–492.
[21] L.M. Rios, N.V. Sahinidis, Derivative-free optimization: A review of algorithms and comparison of software implementations, J. Glob. Optim. 56 (3) (2013) 1247–1293.

[22] J.W. Kim, S. Jung, J. Kim, T.W. Seo, Hybrid Taguchi-Random Coordinate Search Algorithm for Global Numerical Optimization Problems, 2015 (Manuscript submitted for publication).
[23] S. Dibakar, T.S. Mruthyunjaya, Synthesis of workspaces of planar manipulators with arbitrary topology using shape representation and simulated annealing, Mech. Mach. Theory 34 (3) (1999) 391–420.
[24] H. Zhou, E.H. Cheung, Optimal synthesis of crank–rocker linkages for path generation using the orientation structural error of the fixed link, Mech. Mach. Theory 36 (8) (2001) 973–982.
[25] J.W. Kim, J. Bak, T. Seo, J. Kim, New Angular Transmission Design Based on a Four-Bar Linkage Mechanism, Proc. of ASME IDETC, Aug. 2–5, Boston, 2015.